nature physics

REVIEW ARTICLE

PUBLISHED ONLINE: 3 OCTOBER 2012 | DOI: 10.1038/NPHYS2438

Magnetism and its microscopic origin in iron-based high-temperature superconductors

Pengcheng Dai[1,2]*, Jiangping Hu[2,3] and Elbio Dagotto[1,4]*

High-temperature superconductivity in the iron-based materials emerges from, or sometimes coexists with, their metallic or insulating parent compound states. This is surprising, as these undoped states exhibit dramatically different antiferromagnetic spin arrangements and Néel temperatures. Although there is a general consensus that magnetic interactions are important for superconductivity, much remains unknown concerning the microscopic origin of the magnetic states. In this review, we summarize the progress in this area, focusing on recent experimental and theoretical results, and their microscopic implications. We conclude that the parent compounds are in a state that is more complex than that implied by a simple Fermi surface nesting scenario, and a dual description including both itinerant and localized degrees of freedom is needed to properly describe these fascinating materials.

Soon after the discovery of high critical-temperature (high-T_c) superconductivity in copper oxides[1], neutron scattering studies revealed that the parent compounds of these superconductors have an antiferromagnetic (AF) ground state with a simple collinear spin structure (Fig. 1a)[2,3]. Because the associated AF spin fluctuations may be responsible for electron pairing and superconductivity[4–6], over the past 25 years a tremendous effort has focused on characterizing the interplay between magnetism and superconductivity in these materials[7]. In the undoped state, the parent compounds of copper oxide superconductors are Mott insulators and have exactly one valence fermion with spin 1/2 for each copper atom, leading to robust electronic correlations and localized magnetic moments[5,6]. Superconductivity emerges after introducing charge carriers that suppress the static AF order. Although the strong Coulomb repulsion in the parent compounds is screened by the doped charge carriers, the electronic correlations are certainly important for the physics of the doped cuprates, particularly in the underdoped regime[6].

Consider now the iron-based superconductors[8–10]. Several parent compounds of these materials, such as LaFeAsO, $BaFe_2As_2$, NaFeAs and FeTe, are not insulators but semimetals[11–14]. In these cases, electronic band structure calculations have revealed that their Fermi surfaces (FSs) are composed of nearly cylindrical hole and electron pockets at the $\Gamma(0,0)$ and $M(1,0)/M(0,1)$ points, respectively[15,16]. The high density of states (DOS) resulting from the extended momentum space with nearly parallel FS between the hole and electron pockets leads to an enhancement of the particle–hole susceptibility. This suggests that FS nesting among those pockets could induce spin-density-wave (SDW) order at the in-plane AF wave vector $\mathbf{Q}_{AF} = (1,0)$ with a collinear spin structure (Fig. 1b)[17], much like the FS-nesting-induced SDW in pure chromium[18]. Neutron scattering experiments on LaFeAsO (ref. 19), $BaFe_2As_2$ (ref. 20) and NaFeAs (ref. 21) have reported results compatible with the theoretically predicted AF spin structure, albeit with an ordered magnetic moment smaller than expected from first-principles calculations[22]. In addition, quasiparticle excitations between the hole and electron FS can induce $s^{\pm}$-wave superconductivity[15,16,23–25]. One of the consequences of this superconducting state is that the imaginary part of the dynamic susceptibility, $\chi''(Q,\omega)$, should have a sharp peak, termed spin resonance in copper oxide superconductors[26], at $\mathbf{Q}_{AF} = (1,0)$ below T_c (refs 27,28). This prediction is also confirmed by inelastic neutron scattering (INS) experiments in iron-based superconductors such as hole-doped $Ba_{1-x}K_xFe_2As_2$ (refs 29–31), electron-doped $BaFe_{2-x}T_xAs_2$ (T = Co, Ni; refs 32–38) and $FeTe_{1-x}Se_x$ (refs 39–41). Finally, angle resolved photoemission spectroscopy (ARPES) experiments find that the general characterization of the FS and the superconducting order parameter are consistent with the band structure calculations and with isotropic s-wave superconducting gaps[42]. Therefore, at first sight it may seem that antiferromagnetism in the iron-based materials originates from FS nesting of itinerant electrons, that superconductivity must have a $s^{\pm}$-wave symmetry for related reasons and that electron correlations or local moments do not play an important role for magnetism and superconductivity[15].

However, although the parent compounds of iron pnictide superconductors have metallic ground states consistent with band structure calculations, there are reasons to believe that electron correlations could be sufficiently strong to produce 'incipient' Mott physics[43,44], where local moments are as important as itinerant electrons for magnetic, transport and superconducting properties in these materials[45,46]. In fact, the $s^{\pm}$ pairing symmetry is also naturally derived in multi-orbital $t-J$-type models[47,48] and recent diagonalization calculations[49] have shown that the AF state, as well as the A_{1g} s-wave pairing state, evolve smoothly from weak to strong coupling, suggesting that the physics of the pnictides could also be rationalized based on short length scale concepts not rooted in weak-coupling nesting. After all, in the context of the copper oxide superconductors, weak coupling studies of the one-orbital Hubbard model also led to the correct chequerboard AF state and d-wave pairing, showing that these problems can be attacked from a variety of viewpoints. In addition, the newly discovered $A_yFe_{2-x}Se_2$ (A = K, Rb, Cs, Tl) iron-chalcogenide superconductors[50,51] do not exhibit

[1]Department of Physics and Astronomy, The University of Tennessee, Knoxville, Tennessee 37996-1200, USA, [2]Beijing National Laboratory for Condensed Matter Physics, Institute of Physics, Chinese Academy of Sciences, PO Box 603, Beijing 100190, China, [3]Department of Physics, Purdue University, West Lafayette, Indiana 47907, USA, [4]Materials Science and Technology Division, Oak Ridge National Laboratory, Oak Ridge, Tennessee 37831, USA.
*e-mail: pdai@utk.edu; edagotto@utk.edu.

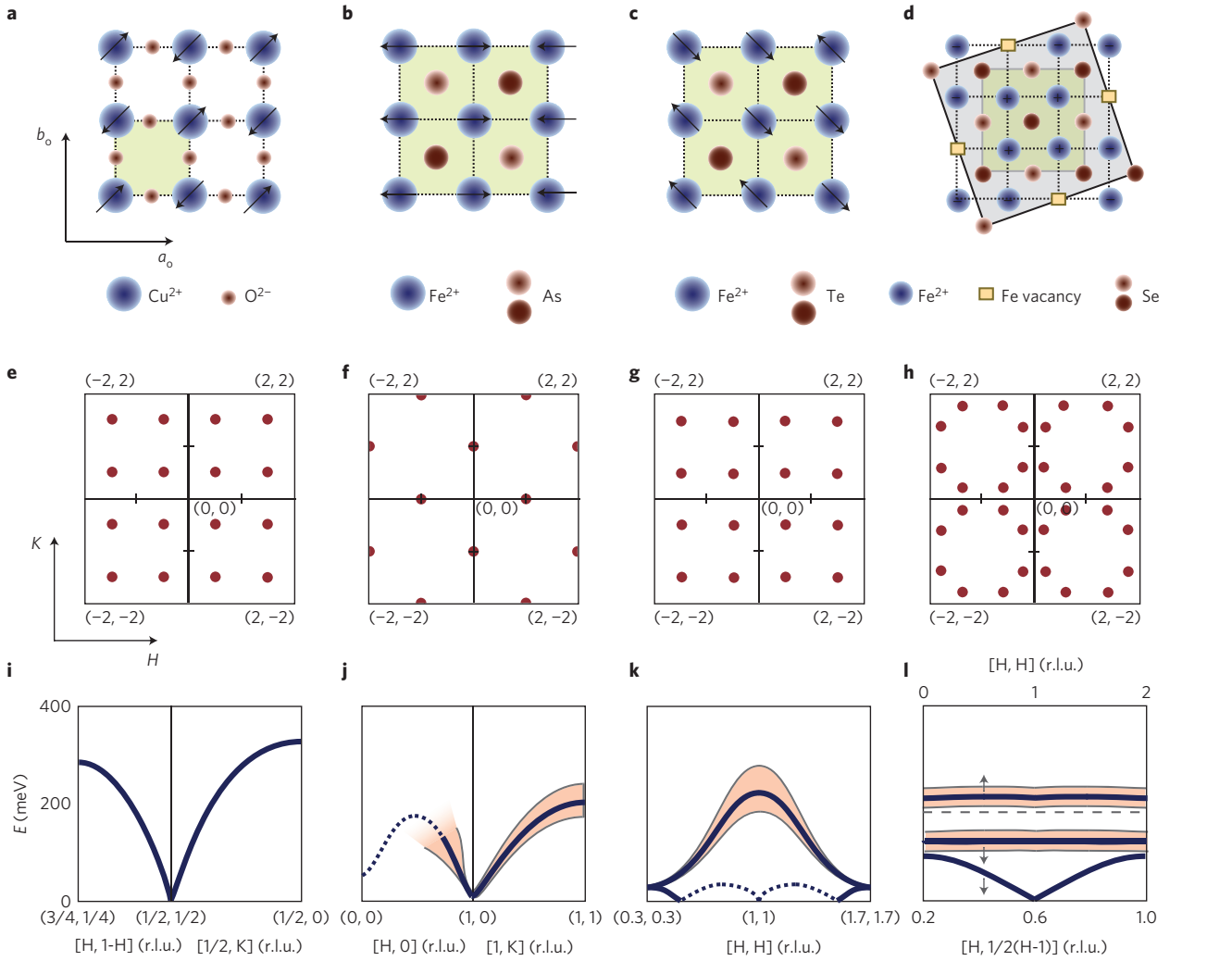

Figure 1 | AF structure and spin-wave dispersions for the insulating copper oxide La_2CuO_4 and the parent compounds of iron-based superconductors $BaFe_2As_2$, FeTe and $A_yFe_{1.6+x}Se_2$. The chemical unit cells are marked light green. The dark and light brown As/Te/Se atoms indicate their vertical positions above and below the Fe-layer, respectively. **a**, The AF structure of La_2CuO_4. **b**, The collinear AF structure of nonsuperconducting iron pnictides in the FeAs-layer, where spins are aligned antiparallel along the orthorhombic a_o-axis[19–21]. **c**, The bi-collinear AF structure of FeTe (refs 63,64). **d**, The block AF order of the insulating $A_yFe_{1.6+x}Se_2$, where the $\sqrt{5}\times\sqrt{5}$ superlattice structure is marked by solid lines with lattice parameter $a_s = 8.663$ Å and the orthorhombic lattice cell is shaded green[55,56]. The iron vacancies are marked as yellow squares. **e**–**h**, The wave vector dependence of the AF order in the (H,K) plane of the reciprocal space for: **e**, La_2CuO_4 (ref. 59); **f**, $BaFe_2As_2$ (ref. 20); **g**, $Fe_{1.05}Te$ (refs 63,64); and **h**, the insulating $A_yFe_{2-x}Se_2$ (refs 55,56). The red circles indicate the positions of the AF Bragg peaks in reciprocal space for different materials. **i**, Spin-wave dispersions along two high-symmetry directions for La_2CuO_4 (ref. 59). The overall energy scale of spin waves for copper oxides is about 320 meV and spin waves are instrumental resolution limited. **j**, Spin-wave dispersions for $BaFe_2As_2$, which broaden considerably for energies above ~100 meV (ref. 68). **k**, Spin-wave dispersions for $Fe_{1.05}Te$, which are very broad for energies above 30 meV (ref. 70). The thick dashed lines in **j**,**k** indicate the expected spin wave dispersions with no magnetic scattering intensity. **l**, Spin waves for the insulating $Rb_{0.89}Fe_{1.58}Se_2$ (ref. 72). The two down arrows indicate wave vector scales for acoustic and low-energy optical spin waves. The up arrow indicates wave vector scales for the high-energy optical waves. The thin dashed line separates the vertical energy scale for the acoustic and low-energy optical spin waves from the high-energy optical spin waves. In spite of the dramatically different dispersions for various iron-based materials, their overall spin-wave energy scales are similar and about 220 meV, less than that of the insulating copper oxides. Twinning is considered.

hole pockets[52–54], but have strong AF ordered insulating phases with extremely high Néel transition temperatures[55,56]. Such a strong magnetism and high superconducting transition-temperature ($T_c \approx$ 33 K) cannot be explained by FS nesting as this is based on the enhancement of the particle–hole susceptibility due to an extended momentum space with nearly parallel FS; that is, it applies only to particle and hole FSs and not to purely electronic Fermi pockets.

Because iron-based superconductors have six electrons occupying the nearly degenerate 3*d* Fe orbitals, the system is intrinsically multi-orbital and therefore it is technically difficult to define and study a simple microscopic Hamiltonian to describe the electronic properties of these materials and characterize the strength of the electronic correlations. From optical conductivity measurements[57], it has been argued that electronic correlations in Fe pnictides are weaker than in underdoped copper oxides, but are stronger than those of Fermi liquid metals, contrary to the conclusion based on local density approximation calculations[15]. Therefore, it is important to determine whether magnetism in Fe-based materials arises from weakly correlated itinerant electrons[15], as in the case of the SDW in chromium[18], or whether it requires some degree of electron correlations[58], or if magnetism is dominated by the contributions of quasi-localized moments induced

Table 1 | Comparison of effective magnetic exchange couplings for parent compounds of copper-based and iron-based superconductors obtained by fitting spin waves with a Heisenberg Hamiltonian with NN (J_{1a}, J_{1b}), NNN (J_{2a}, J_{2b}), and NNNN (J_3).

Parent compounds	T_N (K)	SJ_{1a} (meV)	SJ_{1b} (meV)	SJ_{2a} (meV)	SJ_{2b} (meV)	SJ_3 (meV)
La_2CuO_4 (ref. 59)	317±3	111.8±4	111.8±4	−11.4±3	−11.4±3	0
$CaFe_2As_2$ (ref. 66)	~170	49.9±9.9	−5.7±4.5	18.9±3.4	18.9±3.4	0
$BaFe_2As_2$ (ref. 68)	~138	59.2±2.0	−9.2±1.2	13.6±1	13.6±1	0
$Fe_{1.05}Te$ (ref. 70)	~68	−17.5±5.7	−51.0±3.4	21.7±3.5	21.7±3.5	6.8±2.8
$Rb_{0.89}Fe_{1.58}Se_2$ (ref. 72)	~475	−36±2	15±8	12±2	16±5	9±5

The Néel temperatures T_N for different materials are also listed. Errors indicate one standard deviation.

by incoherent electronic excitations[44], such as in the AF insulating state of copper oxides[6].

In this Review, recent experimental and theoretical progress in the study of iron-based superconductors is summarized, with a focus on the undoped parent compounds. We begin with a discussion of the magnetically ordered states in nonsuperconducting iron pnictides, iron chalcogenides and iron selenides. We then move on to describe the effects of electron and hole doping on static AF order and their associated spin excitations. Next, we provide several examples where deviations from the simple SDW FS nesting picture are prominent. Finally, we present our perspective on the importance of electron correlations in these materials.

Magnetic order and spin waves in the parent compounds

Although the overall crystal structures and chemical formulas of the copper-oxide superconductors can be quite different, their parent compounds are all AF Mott insulators characterized by the Cu spin structure shown in Fig. 1a, where the tetragonal or pseudo-tetragonal unit cells have a nearest-neighbour (NN) Cu–Cu spacing with $a \approx b \approx 3.8$ Å. In the notation of reciprocal lattice units (rlu) $(2\pi/a, 2\pi/b, 2\pi/c)$, the AF Bragg peaks occur at the in-plane ordering wave vectors $\mathbf{Q}_{AF} = (\pm 1/2 + m, \pm 1/2 + n)$, where $m, n = 0, \pm 1, \pm 2, \ldots$ rlu, shown as red circles in Fig. 1e (refs 2,3). Time-of-flight INS experiments[59,60] have mapped out spin waves of the insulating La_2CuO_4 throughout the Brillouin zone and found no evidence for spin-wave broadening at high energies. The dispersions of spin waves are well described by a Heisenberg Hamiltonian with NN exchange coupling $J_1 = 111.8 \pm 4$ meV and next-nearest-neighbour (NNN) exchange $J_2 = -11.4 \pm 3$ meV (ref. 59). Therefore, the dominant magnetic exchange coupling in La_2CuO_4 is the NN magnetic interaction and the higher-order interactions amount to only ~10% of the total magnetic energy with a bandwidth of ~320 meV (Fig. 1i).

In the four years since the initial discovery of superconductivity in $LaFeAsO_{1-x}F_x$ (ref. 11), there are now three major families of iron-based superconductors: the iron pnictides[8,9], iron chalcogenides[14,61] and alkaline iron selenides[50,51]. The parent compounds of the pnictides, such as AFeAsO (A = La, Ce, Sm, Pr, and so on.), AFe_2As_2 (A = Ba, Sr, Ca) and NaFeAs, all have the same collinear AF structure, as shown in Fig. 1b, with a small ordered moment ($< 1\ \mu_B$/Fe) and Néel temperature $T_N \leq 200$ K (refs 13,19, 20). The AF spin moments are aligned along the weak orthorhombic unit cell a-axis direction ($a \approx 5.62$, $b \approx 5.57$ Å). In reciprocal space, the AF Bragg peaks occur at in-plane ordering wave vectors $\mathbf{Q}_{AF} = (\pm 1 + m, n)$ and at $\mathbf{Q}_{AF} \approx (m, \pm 1 + n)$ due to twinning (red circles in Fig. 1f), consistent with the $\Gamma(0,0) \leftrightarrow M(1,0)/M(0,1)$ FS nesting picture[15]. However, although the calculated FS of the chalcogenides $Fe_{1+y}Te_{1-x}Se_x$ is similar to that of iron pnictides[62], surprisingly its parent compound $Fe_{1+y}Te$ actually has a bi-collinear spin structure (Fig. 1c)[63,64]. Here, the AF Bragg peaks occur at $\mathbf{Q}_{AF} = (\pm 1/2 + m, \pm 1/2 + n)$ (Fig. 1g) in the pseudo-tetragonal notation ($a \approx b \approx 5.41$ Å), suggesting that FS nesting cannot induce such AF order. Finally, the parent compounds of the alkaline iron selenide $AFe_{1.6+x}Se_2$ superconductors are insulators[50,51], and form a $\sqrt{5} \times \sqrt{5}$ block AF structure, as shown in Fig. 1d, with a large ordered moment (~3 μ_B/Fe) along the c-axis and $T_N \approx 500$ K (refs 55,56). In reciprocal space, defined using the pseudo-tetragonal unit cell of iron pnictides ($a \approx b \approx 5.41$ Å), the block AF Bragg peaks appear at $\mathbf{Q}_{AF} = (\pm 0.2 + m, \pm 0.6 + n)$ and $(\pm 0.6 + m, \pm 0.2 + n)$, combining left and right chiralities (red circles in Fig. 1h).

As the parent compounds of iron-based superconductors can have different AF spin structures and either metallic or insulating ground states[8,9,50,51], the microscopic origin of the AF order cannot be induced by a simple FS nesting. If magnetism is relevant for high-T_c superconductivity, then it would be important to determine magnetic exchange couplings for different classes of Fe-based superconductors and compare the results with those of the copper oxides[59]. For pnictides, INS experiments have mapped out spin waves on single crystals of $CaFe_2As_2$ (refs 65,66), $SrFe_2As_2$ (ref. 67) and $BaFe_2As_2$ (ref. 68) throughout the Brillouin zone. Although there are still debates concerning whether spin waves in these materials can be described by a pure itinerant picture[65,67] or require local moments[66,68], the overall spin-wave energy scales are around 220 meV. Therefore, magnetic exchange couplings in iron pnictides are clearly smaller than those of copper oxides (Fig. 1i,j). Although spin waves are broadened at high energies, the spin-wave dispersion curves (Fig. 1j) can still be described by a Heisenberg Hamiltonian with strong anisotropic NN exchange couplings ($J_{1a} \gg J_{1b}$) and fairly large NNN exchange coupling (J_2; refs 66,68). This large in-plane magnetic exchange coupling anisotropy has been interpreted as being due to a possible electronic nematic phase and/or orbital ordering[66,68]. Table 1 compares the effective magnetic exchange couplings of the Fe-based systems studied thus far against those of the insulating copper oxide La_2CuO_4.

For the chalcogenides $Fe_{1+y}Te$, the commensurate bi-collinear AF spin structure in Fig. 1c becomes incommensurate for concentration $y > 0.12$ (ref. 69). The overall spin-wave energy scale (Fig. 1k) is similar to those of the iron pnictides. Although the large static ordered moment of ~2 μ_B/Fe in $Fe_{1+y}Te$ (refs 63,64) suggests that local moments may be important, spin waves are rather broad in energy and difficult to fit using a Heisenberg Hamiltonian with only NN and NNN exchange couplings[70]. By including third-neighbour (NNNN) exchange couplings, a Heisenberg Hamiltonian can fit the spin-wave dispersion with an anisotropic ferromagnetic NN exchange couplings and strong AF NNN exchange coupling (Table 1). In a separate INS experiment on $Fe_{1.1}Te$, the total integrated Fe magnetic moment was found to increase with increasing temperature from 10 to 80 K (ref. 71). These results suggest that in the temperature range relevant for superconductivity, there is a remarkable redistribution of the magnetism arising from both itinerant and localized electrons.

In the case of insulating $AFe_{1.6+x}Se_2$, spin waves have an acoustic mode and two optical modes separated by spin gaps (Fig. 1l)[72]. In contrast to iron pnictide AFe_2As_2 (refs 65–68) and iron chalcogenide $Fe_{1+y}Te$ (refs 70,71), spin waves in insulating

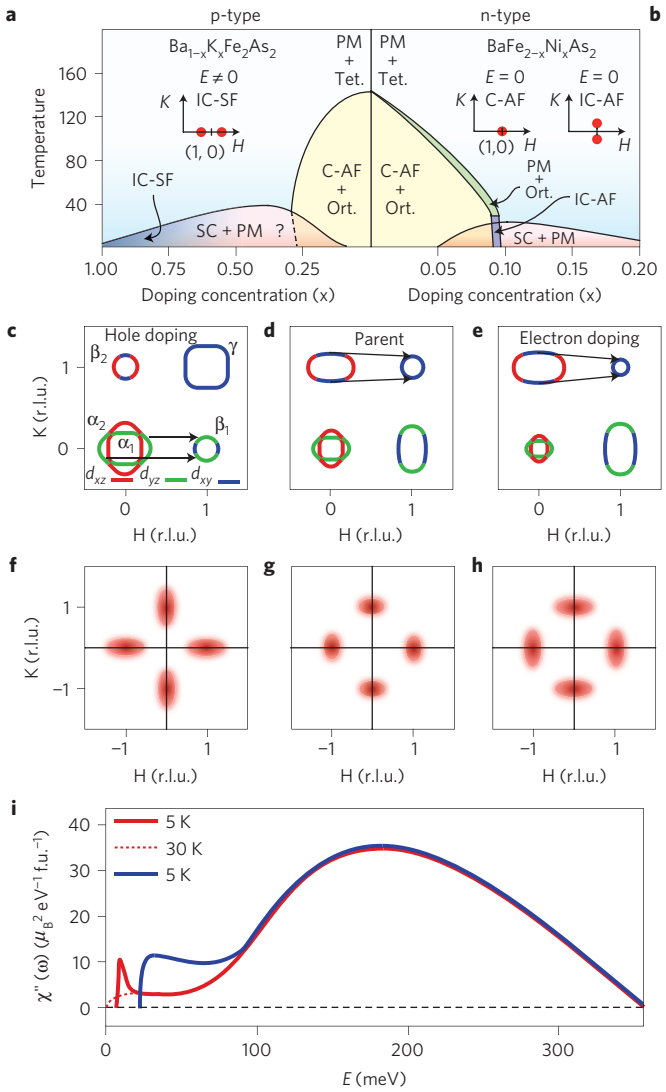

Figure 2 | The electronic phase diagrams and the evolution of FSs, static AF order and spin excitations on electron or hole doping to $BaFe_2As_2$. **a**, The AF and superconducting phase diagram for hole-doped $Ba_{1-x}K_xFe_2As_2$. In the underdoped regime, there is a region of coexisting AF order and superconductivity[86]. Incommensurate spin excitations appear for $x \geq 0.4$ (ref. 31) and persist till $x = 1$ at KFe_2As_2 (ref. 90). The inset shows the longitudinal incommensurate spin fluctuations for KFe_2As_2 (ref. 90). **b**, Phase diagram for electron-doped $BaFe_{2-x}Ni_xAs_2$ (ref. 81). The long commensurate AF order changes into short-range incommensurate AF order near $x = 0.092$. The right inset shows the transverse incommensurate AF order. The left inset shows the static commensurate AF order present for $x \leq 0.085$ (ref. 81). Superconductivity in the electron-doped materials only extends to $x \approx 0.25$. **c**, Schematics of FSs correspond to 35% hole-doped $BaFe_2As_2$ (ref. 30) with possible nesting vectors marked with arrows. The d_{xz}, d_{yz}, and d_{xy} orbitals for different FSs are coloured as red, green and blue, respectively. **d**, FSs of $BaFe_2As_2$ with orbital characters[87]. **e**, FS of 8% electron-doped $BaFe_2As_2$ (ref. 30). For all three cases shown in **c**–**e**, FSs are plotted with zero wave vector transfers along the *c*-axis. **f**, Longitudinally elongated spin excitations at $E = 20$ meV seen in the optimally hole-doped $Ba_{0.67}K_{0.33}Fe_2As_2$ (ref. 30). **g**, Transversely elongated spin waves at $E = 20$ meV for $BaFe_2As_2$ (ref. 68). **h**, Transversely elongated spin excitations at $E = 20$ meV for $BaFe_{1.9}Ni_{0.1}As_2$ (refs 35,89). **i**, Energy dependence of $\chi''(\omega)$ for $BaFe_2As_2$ (blue solid line) and $BaFe_{1.9}Ni_{0.1}As_2$ below (red dashed line) and above (red solid line) T_c in absolute units of μ_B^2 eV^{-1} f.u.$^{-1}$. The sharp peak near $E \approx 8$ meV below T_c is the neutron spin resonance coupled directly to superconductivity[32–38].

$AFe_{1.6+x}Se_2$ can be described well by a Heisenberg Hamiltonian with NN, NNN and NNNN exchange couplings[72]. Comparing effective exchange couplings for different iron-based materials (Table 1), it is clear that the NN exchange couplings are quite different, but the NNN exchange couplings are AF and rather similar. In addition, spin waves for iron-based materials are much broader at high energies. This is different from the insulating copper oxides, where the NN exchange coupling dominates the magnetic interactions and spin waves are limited by instrumental resolution throughout the Brillouin zone[59,60]. These results suggest that itinerant electrons play a role in the spin waves of metallic iron-based materials.

The effects of doping on the magnetic state

As discussed before[8–10], superconductivity in Fe-based materials can be induced via electron/hole doping, pressure and isoelectronic substitution. Figure 2a,b show the electronic phase diagrams of hole and electron doping on $BaFe_2As_2$, respectively. In the undoped state, $BaFe_2As_2$ exhibits simultaneous structural and magnetic phase transitions below ~138 K, changing from the high-temperature paramagnetic tetragonal phase to the low-temperature orthorhombic phase with the collinear AF structure (Fig. 1b)[20]. On electron-doping $BaFe_2As_2$ by partially replacing Fe by Co or Ni to form $BaFe_{2-x}T_xAs_2$, the static AF order is suppressed and superconductivity emerges[8–10]. From systematic transport and magnetic measurements of single crystals[73,74], the phase diagram for $BaFe_{2-x}Co_xAs_2$ was established, where the single structural/magnetic phase transition in $BaFe_2As_2$ splits with increasing Co-doping. Neutron diffraction experiments on $BaFe_{2-x}Co_xAs_2$ (ref. 75) confirm that the commensurate AF order appears below the structural transition temperature and superconductivity coexists with AF order for $0.06 \leq x \leq 0.102$. Neutron scattering measurements on $BaFe_{2-x}Co_xAs_2$ with coexisting AF order and superconductivity reveal that the intensity of AF Bragg peaks actually decreases below T_c without changing the spin–spin correlation lengths[76,77]. Although these results indicate that the static AF order competes with superconductivity, it remains unclear whether the long-range AF order truly coexists microscopically with superconducting regions[78,79]. Recently, for electron-doped samples near optimal superconductivity, it has been shown that the commensurate static AF order changes into transversely incommensurate short-range AF order that coexists and competes with superconductivity (see inset in Fig. 2b)[80,81]. Taking the temperature dependence of the orthorhombic lattice distortion of $BaFe_{2-x}Co_xAs_2$ into account[82], the AF order, structure and superconductivity phase diagrams for $BaFe_{2-x}T_xAs_2$ are shown in Fig. 2b.

Although the superconducting transition temperature for hole-doped $Ba_{1-x}K_xFe_2As_2$ can reach up to $T_c = 38$ K (ref. 12), as compared with the $T_c \approx 25$ K for electron-doped $BaFe_{2-x}T_xAs_2$ (refs 8,9), these materials are much less studied because of the difficulty of growing high-quality single crystals. The initial transport and neutron scattering experiments on powder samples indicated a gradual suppression of the concurrent structural and magnetic phase transitions with increasing K-doping. For the underdoped regime $0.2 \leq x \leq 0.4$, commensurate AF order seems to microscopically coexist with superconductivity[83]. Subsequent neutron scattering and muon spin rotation (μSR) measurements on single crystals grown in Sn-flux suggested mesoscopic separation of the AF and superconducting phases[84]. However, recent neutron[85], X-ray scattering and μSR work[86] on high-quality powder samples confirm the microscopic coexistence of the commensurate AF order with superconductivity in the underdoped region between $0.2 \leq x \leq 0.3$ and the suppression of the orthorhombic phase below T_c (Fig. 2a). As at present there is no neutron diffraction work on high-quality single crystals of $Ba_{1-x}K_xFe_2As_2$ grown using FeAs-flux, it is unclear if there is also short-range incommensurate AF order in $Ba_{1-x}K_xFe_2As_2$ near optimal superconductivity.

The appearance of static incommensurate AF order along the transverse direction of the collinear AF ordering wave vector $\mathbf{Q}_{AF} = (\pm 1, 0)$ in $BaFe_{2-x}T_xAs_2$ suggests that such order arises from the electron doping effect of FS nesting[80,81]. Based on a five-orbital tight-binding model, fitted to the density functional theory (DFT) band structure for $BaFe_2As_2$ (ref. 87), there should be five FS pockets with different orbital contributions in the two-dimensional reciprocal space at $\mathbf{Q}_z = 0$ (Fig. 2d). The intraorbital, but interband, scattering process between $\Gamma(0,0) \leftrightarrow M(1,0)$ shown in Fig. 2d favours the transversely lengthened vertices[88]. This momentum anisotropy is compatible with the experimentally observed elliptically shaped low-energy spin excitations in superconducting $BaFe_{2-x}T_xAs_2$ (refs 35–38) and spin waves in $BaFe_2As_2$ (Fig. 2g)[68]. On electron-doping to enlarge the electron pockets near $M(1,0)/(0,1)$ and to shrink the hole pockets near $\Gamma(0,0)$, the mismatch between the electron and hole Fermi pockets becomes larger (Fig. 2e), resulting in a more transversely elongated ellipse in the low-energy magnetic response (Fig. 2h). Indeed, this is qualitatively consistent with the doping evolution of the low-energy spin excitations[35,38,89].

For hole-doped $Ba_{1-x}K_xFe_2As_2$, one should expect enlarged hole Fermi pockets near $\Gamma(0,0)$ and reduced electron pockets near $M(1,0)/(0,1)$, as shown in Fig. 2c. Based on first-principles calculations, spin excitations for optimally hole-doped $Ba_{1-x}K_xFe_2As_2$ at $x = 0.4$ should have longitudinally elongated ellipses[35], and gradually evolve into incommensurate magnetic scattering (elastic and/or inelastic) with increasing x because of poor nesting between the hole and electron Fermi pockets[31]. INS experiments on single crystal $Ba_{0.67}K_{0.33}Fe_2As_2$ (ref. 30) indeed confirm that the low-energy spin excitations are longitudinally elongated ellipses that are rotated 90° from that of the electron-doped $BaFe_{2-x}T_xAs_2$ (Fig. 2f)[35–38]. Furthermore, INS measurements on powder samples of $Ba_{1-x}K_xFe_2As_2$ reveal that spin excitations change from commensurate to incommensurate for $x \geq 0.4$, although their exact line shape and incommensurability in reciprocal space are unknown[31]. Finally, INS experiments on hole-overdoped KFe_2As_2 found incommensurate spin fluctuations along the longitudinal direction (inset in Fig. 2a), again consistent with the FS nesting picture[90]. Figure 2a shows the electronic phase diagram of hole-doped $Ba_{1-x}K_xFe_2As_2$ based on the present understanding of these materials.

Although FS nesting is compatible with a number of experimental observations of the evolution of spin excitations in electron/hole-doped iron-based superconductors, there are several aspects of the problem where such a scenario cannot be reconciled with experiments. In a recent INS experiment on optimally electron-doped $BaFe_{1.9}Ni_{0.1}As_2$, magnetic excitations throughout the Brillouin zone have been measured in absolute units and compared with spin waves for AF $BaFe_2As_2$ (ref. 89). In the fully localized (insulating) case, the formal Fe^{2+} oxidation state in $BaFe_2As_2$ would give a $3d^6$ electronic configuration and Hund's rules would yield $S = 2$. The total fluctuating moments should be $\langle m^2 \rangle = (g\mu_B)^2 S(S+1) = 24\ \mu_B^2$ per Fe assuming $g = 2$ (refs 36,89). For spin waves in the insulating $Rb_{0.89}Fe_{1.58}Se_2$, the total moment sum rule seems to be satisfied[72]. The fluctuating moments for $BaFe_2As_2$ and $BaFe_{1.9}Ni_{0.1}As_2$ are $\langle m^2 \rangle = 3.17 \pm 0.16$ and $3.2 \pm 0.16\ \mu_B^2$ per Fe(Ni), respectively[89]. Although these values are considerably smaller than those of the fully localized case, they are much larger than expected from the fully itinerant SDW using the random phase approximation[91]. A calculation combining DFT and dynamical mean field theory (DMFT) suggests that both the band structure and the local moment aspects (for example Hund's coupling) of the iron electrons are needed for a good description of the magnetic responses[89]. Figure 2i shows the energy dependence of $\chi''(\omega)$ for $BaFe_2As_2$ and $BaFe_{1.9}Ni_{0.1}As_2$, and it is clear that the impact of electron doping and superconductivity are limited to spin excitation energies below 100 meV. These results suggest that high-energy spin excitations are likely to arise from the local moments instead of FS nesting effects.

Deviations from the simple SDW FS nesting picture

After the early research efforts on Fe-based superconductors[8–10], recent experimental and theoretical investigations are providing a more refined perspective of these materials. Below, several selected examples will be discussed, supplementing those presented in the previous sections.

Strength of electronic correlations. The strength of electronic correlations is often characterized by means of the ratio between the on-site Hubbard repulsion coupling U and the bandwidth W of the hole or electron carriers. Early on, it was assumed that pnictides were in the weak-interaction limit $U/W \ll 1$. However, recent investigations revealed that the electronic correlations induce large enhancements between the effective and bare electronic masses, signalling that correlation effects cannot be neglected. For instance, Haas–van Alphen experiments for KFe_2As_2 revealed discrepancies between the band-theory calculated and observed FSs, including a large electronic mass enhancement 3–7 caused by band narrowing[92]. Similar ratios for the overdoped $Tl_2Ba_2CuO_{6+\delta}$ copper-oxides have been reported[93], suggesting that the undoped parent compounds of the pnictides resemble the overdoped copper oxides.

Further insight is provided by optical conductivity experiments, as the ratio R between the experimentally measured kinetic energy and that of band-theory calculations can be measured and contrasted against other compounds[57]. $R \approx 1$ signals a good metal such as silver. LaFePO presents a ratio $R \approx 0.5$, which is borderline between weak and moderate coupling. However, pnictides such as $BaFe_{2-x}T_xAs_2$ are characterized by an even stronger correlation, which induces a ratio $R \approx 0.3$, similar to results for overdoped $La_{2-x}Sr_xCuO_4$, widely considered to be a 'correlated metal'. Other studies have arrived at similar conclusions with regard to the correlation strength[94,95]. In agreement with experiments, DFT + DMFT predicts a mass enhancement $m^*/m_{band} \sim 2$–3 for $BaFe_{2-x}T_xAs_2$ and ~7 for FeTe (ref. 96). Moreover, ARPES studies of NaFeAs revealed band reconstructions in the magnetic state involving bands well below the FS (ref. 97), contrary to a weak coupling picture.

Hubbard model investigations provide further insight into this subject. When compared with similar efforts for the cuprates, the study of Hubbard models for the pnictides is far more challenging because several Fe orbitals are needed. For this reason, many efforts are restricted to mean-field Hartree–Fock approximations. For the undoped three-orbital Hubbard model, employing the d_{xz}, d_{yz}, and d_{xy} orbitals of relevance at the FS, a sketch of a typical mean-field phase diagram varying U and the Hund coupling J_H (ref. 98) is shown in Fig. 3a. Three regimes are identified: a small-U phase, where the state is paramagnetic, followed with increasing U by an intermediate regime, simultaneously metallic and magnetic[98] and finally a large-U phase, where a gap in the density-of-states is induced, leading to an insulator (with concomitant orbital order). Comparing the theoretical predictions for the magnetic moment in the $\mathbf{Q}_{AF} = (1,0)$ wave-vector channel against neutrons, and the one-particle spectral function $A(\mathbf{k},\omega)$ against ARPES, the intermediate-coupling region, dubbed 'physical region' in yellow in Fig. 3a, represents qualitatively the undoped $BaFe_{2-x}T_xAs_2$ compounds[98]. In this regime, $U/W \sim 0.3$–0.4, and similar results were reported for the two- and five-orbital models[99]. Note that Hartree–Fock usually produces critical couplings smaller than they truly are because of the neglect of quantum fluctuations. In fact, recent investigations beyond Hartree–Fock[100] suggest that the relevant U may be larger than those found in Hartree–Fock[98] by approximately a factor of two. The study of effective low-energy Hamiltonians starting from first-principles calculations also led to the conclusion that U/W is between 0.5 and 1.0 for the pnictides, depending on the particular compound[101]. Thus, the regime of relevance is neither

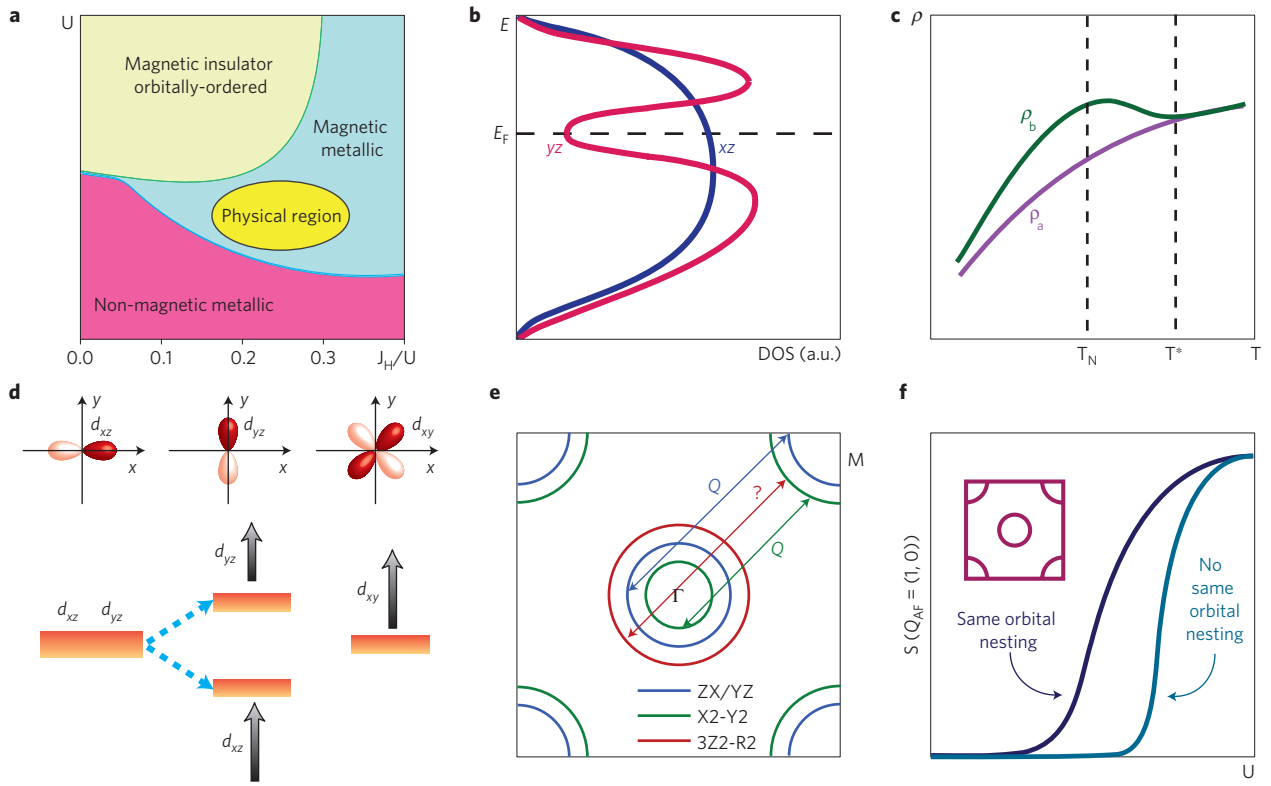

Figure 3 | Summary of the phase diagram of multiorbital Hubbard models and the electronic state of Fe near the FS. a, Sketch of the phase diagram of a typical multiorbital Hubbard model in the undoped limit, varying the on-site same-orbital repulsion U and the ratio between the Hund coupling J_H and U. Highlighted is a region dubbed 'physical region' where the properties of the model are in good agreement with experiments. Note the location of this region in the intermediate magnetic-metallic phase, with magnetic order at $\mathbf{Q}_{AF} = (1, 0)$, at similar distance from the paramagnetic state and from the orbitally ordered insulating state[98]. **b**, Sketch of the DOS illustrating the phenomenon of FS orbital order, which is a weight redistribution at the FS of the states associated with the *xz* and *yz* *d*-orbitals. Even though the integral over energy gives similar values for both orbitals, at the FS there are drastic differences that influence several properties, such as transport[107,129]. **c**, Sketch of the anisotropy found in transport experiments for detwinned $Ba(Fe_{1-x}Co_x)_2As_2$. Note that this anisotropy is present at temperatures substantially larger than T_N (ref. 108). **d**, Orbitals of relevance for the discussion of the Fe-based superconductors and their splitting at the FS. **e**, Sketch of the ARPES results of ref. 120, illustrating the absence of a nesting partner for one of the hole pockets. The material still exhibits a nearly uniform superconducting gap at this and all the other hole and electron pockets. **f**, Sketch of the magnetic moment at wave vector $\mathbf{Q}_{AF} = (1, 0)$ for two models. On the left is the result for a traditional model of pnictides, with the *xz*, *yz*, and *xy* *d*-orbitals active at the FS. This model exhibits magnetic order in a broad range of couplings from very weak to strong. On the right, results of a model with the same FS but totally different orbital composition. Although at small U there is no order, at larger couplings this model converges to the same $\mathbf{Q}_{AF} = (1, 0)$ order[122]. The inset is a sketch of the Fermi surface common to both models, but with very different orbital composition (not shown).

very weak coupling nor strong coupling, but the more subtle, and far less explored, intermediate region. Previous efforts converged to similar conclusions[102]. This is also compatible with the notion that the parent compound is close to a Mott insulator[43,44]. In the 'physical region' the ratio J_H/U is approximately 1/4 (ref. 98), as in other estimations[96], highlighting the importance of J_H in these materials, which are sometimes referred to as Hund metals[103]. Finally, it is very important to note that the above-described analysis of U/W holds for pnictides, but the recent discovery of the alkaline iron selenides[50,51] has opened a new chapter in this field and it is conceivable that for these materials U/W will be larger than in pnictides, explaining, for example, the large values of the iron moments.

Role of the orbital degree of freedom. The 'physical region' in Fig. 3a is not only close to the paramagnetic regime, but also similarly close to the insulator, which in the mean-field approximation is also orbitally ordered[99]. The potential relevance of the orbital degree of freedom in pnictides has been discussed[104,105]. The orbital can be of relevance not only in its long-range-ordered form, but also via its coupling to the spin and its influence near the FS. In fact, polarized ARPES experiments on $BaFe_2As_2$ (ref. 106) reported that at the FS there was an asymmetry between the populations of the d_{xz} and d_{yz} orbitals. Theoretical studies showed that this effect indeed occurs in the $\mathbf{Q}_{AF} = (1, 0)$ magnetic state, and it is linked to an orbital-dependent reduction in the DOS at the FS (ref. 107), sketched in Fig. 3b, a phenomenon dubbed 'Fermi surface orbital order'.

This effect, although not sufficiently strong to induce long-range order as in manganites, can still severely influence the properties of the material. Consider for example the transport anisotropy observed in detwinned $BaFe_{2-x}T_xAs_2$ single-crystals[108,109], sketched in Fig. 3c. At low temperatures the difference between the *a*-axis (spins antiparallel, Fig. 1b) and *b*-axis (spin parallel, Fig. 1b) directions can be rationalized based on the magnetic state, as the different spin arrangements along the *a* and *b* break rotational invariance[110]. However, both in the undoped case and particularly in the lightly doped regime, the asymmetry persists well above the Néel temperature, T_N, into a new temperature scale T^* that may be associated with the onset of nematic order[45,46], similarly as in some ruthenates and copper oxides[111]. ARPES experiments on the same materials[112] reported a d_{xz} and d_{yz} band splitting (Fig. 3d) that occurs above T_N in the same region where transport anisotropies were found. Although the splitting is too small to be a canonical long-range orbital order, it reveals the importance of

fluctuations above the critical temperatures. Optical spectra studies also revealed anisotropies in the spectra persisting up to 2 eV, incompatible with SDW scenarios[113]. Note that the discussion on this subject is still fluid. Although neutron diffraction investigations showed that T_N actually substantially increases as the pressure needed to detwin the crystals increases, potentially explaining the observed resistivity anisotropies[114], magnetic torque measurements without external pressure revealed clear evidence for electronic nematicity[115]. Recent calculations addressing transport indeed find an important role of the orbital states above T_N (ref. 116). The orbital degree of freedom, closely entangled to the spin and the lattice, may lead to a more complex 'normal' state than anticipated from weak coupling, particularly because of the FS orbital order[107]. In fact, neutron scattering shows that although the low-energy magnetic excitations change substantially when crossing critical temperatures, the higher energy features remain the same over a large doping and temperature range[89], suggesting that spin, orbital and lattice are closely entangled. Establishing who is the 'driver' and who is the 'passenger' may define an important area of focus of future research.

Local moments at room temperature. Another deviation from a simple weak coupling picture is the observation of local magnetic moments at room temperature. Within the SDW scenario, magnetic moments are formed on cooling, simultaneously with the development of long-range magnetic order. However, recent Fe X-ray emission spectroscopy experiments have revealed the existence of local moments in the room-temperature paramagnetic state[117]. In fact, with the sole exception of FeCrAs, for all the pnictides and chalcogenides investigated a sizeable room temperature magnetic moment was found. This includes LiFeAs, which actually does not order magnetically at any temperature[13], and $AFe_{1.6+x}Se_2$ with a regular arrangement of Fe vacancies (Fig. 1d). These observed local moments are similar in magnitude to those reported in the low-temperature neutron scattering experiments reviewed in previous sections. Similar conclusions to those of ref. 117 were reached in a study of 3*s* core level emission for $CeFeAsO_{0.89}F_{0.11}$ (ref. 118) and also in LDA+DMFT investigations[119].

Polarized ARPES results and orbital composition. Although research using ARPES techniques applied to pnictides has already been reviewed[42], some intriguing recent results addressing the influence of nesting are included in our discussion. Using bulk-sensitive laser ARPES on $BaFe_2(As_{0.65}P_{0.35})_2$ and $Ba_{0.6}K_{0.4}Fe_2As_2$, an orbital-independent superconducting gap magnitude was found for the hole-pocket FSs (ref. 120). These results are incompatible with nesting, where the FS nested portions must have a robust component of the same orbital to be effective. Actually, the hole pocket shown in red in the sketch in Fig. 3e, which experimentally exhibits a robust and nearly wave-vector-independent superconducting gap, similar to those found in the other hole pockets, does not have a matching electron pocket with the same orbital composition and, thus, it cannot develop its superconductivity via a nesting pairing mechanism[15]. Perhaps interorbital pairing[121] or orbital fluctuations could be relevant to explain this paradox. Recent theoretical work[122] addressed the importance of orbital composition via two models: one with a nested electron-pocket and hole-pocket FS with the standard orbital composition of pnictide models, and another with the same FS shape but with electron and hole pockets having totally different orbital compositions. As sketched in Fig. 3f, the former develops magnetic order at smaller values of U than the latter. However, with sufficiently large U both have magnetic ground states with the same wave vector $\mathbf{Q}_{AF} = (1,0)$ (Fig. 3f). At large U it is clear that the $\mathbf{Q}_{AF} = (1,0)$ order can be understood within a local picture, based on the similar magnitude of the super-exchange interactions between NN and NNN spins using a simple Heisenberg model.

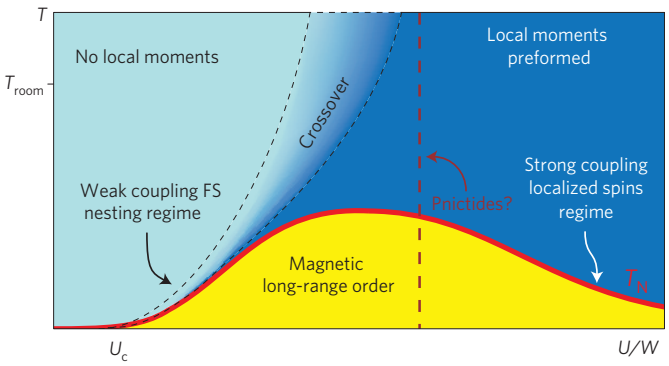

Figure 4 | Sketch of the expected phase diagram of the Hubbard model with varying temperature and U/W in the undoped limit. Highlighted are the regimes of weak coupling, where nesting dominates, and strong coupling, where localized spins approaches are suitable. At temperatures above T_N, there are regions with and without preformed local moments. The vertical dashed line tentatively locates the pnictides in the 'middle', with a physics involving itinerant electrons coexisting with localized moments. The cases of chalcogenides and alkaline iron selenides (not shown) may require a larger U/W. Note that this phase diagram is guided by results known for the one-orbital case, whereas the true multiorbital Hubbard model phase diagram may exhibit an even richer structure. In particular, a second critical U/W at low temperatures separating the metallic AF state from the insulating AF state is not shown for simplicity.

Further experimental results. De Haas–van Alphen studies[123] in non-superconducting $BaFe_2P_2$, the endmember of the superconducting series $BaFe_2(As_{1-x}P_x)_2$, indicate that the differences in the pairing susceptibility with varying x are caused by increases in U and J_H rather than improved geometric nesting. Moreover, ARPES studies of LiFeAs, without long-range magnetic order at low temperatures, report a strong renormalization of the band structure by a factor ~3 and the absence of nesting[124]. Yet, at $T_c = 18$ K (ref. 13) LiFeAs still becomes superconducting, suggesting that nesting is not necessary for superconductivity to develop. Similarly, ARPES experiments on superconducting $AFe_{1.6+x}Se_2$ (refs 53,54,125) revealed the absence of the hole-like FSs necessary for the $\Gamma(0,0) \leftrightarrow M(1,0)$ $s^{\pm}$-wave superconductivity. Also note that related materials such as LaFePO with a well-nested FS also do not order magnetically. Why would weak coupling arguments work in some cases and not others? Finally, scanning tunnelling microscopy experiments[126] on $Ca(Fe_{1-x}Co_x)_2As_2$ show an exotic 'nematic' electronic structure, similar to those found for strongly coupled copper oxides.

Further theoretical results. In fluctuation-exchange approximation studies it was concluded that the nesting results are not robust against the addition of self-energy corrections[127]. Other calculations have suggested that magnetic order in pnictides is neither fully localized nor fully itinerant: the J_H coupling forms the local moments, whereas the particular ground state is selected by itinerant one-electron interactions[102]. Moreover, studies of a spin-fermion model for the pnictides[104,105] revealed the crucial role played by the Hund's rule coupling and suggested that the Fe superconductors are closer kin to manganites, where similar spin-fermion models were extensively studied[128], than to copper oxides with regard to their diverse magnetism and incoherent normal-state electron transport.

Conclusions

Recent studies of Fe-based superconductors are revealing a perspective of these exciting materials that is far richer than previously anticipated. Although in the early days, weak coupling approaches seemed sufficient to understand these compounds, several recent efforts, reviewed in part here, suggest that understanding the physics of these materials may require more refined concepts,

better many-body theoretical calculations and further sophisticated experiments for a more in-depth rationalization of their properties. In fact, evidence is building that pnictides and chalcogenides inhabit the mostly unexplored 'intermediate' region of Hubbard U/W couplings, which is neither very weak coupling, where FS nesting concepts apply, nor strong coupling, where localized spins provide a good starting point, as occurs in the undoped copper oxides. The situation is qualitatively summarized in Fig. 4, where a crude sketch of a plausible phase diagram for a generic undoped Hubbard model is provided for varying temperature T and U/W at, for example, a fixed J_H/U such as 1/4. In weak coupling, first a critical value of U must be crossed before magnetic order develops at low temperatures. In this region, nesting works properly. As U increases, T_N first increases, reaches a broad maximum, and then eventually in the regime of localized spins T_N starts to decrease, as it becomes regulated by the Heisenberg superexchange, which scales as $1/U$. Above T_N, a 'crossover' temperature that roughly grows like U is shown, separating regions with and without 'preformed' local moments. Because the pnictides have local moments at room temperature, a tentative location for these materials is provided by the vertical dashed line. However, whether this line coincides with the maximum T_N or is shifted to the left or the right is too early to say; but it cannot be too far from optimal otherwise local moments would be absent, if far left, or an insulator should be found at low temperatures, if far right. Theoretical mean-field estimates reviewed here using the multiorbital Hubbard model find that $U/W \sim 0.3$–0.5 could work for pnictides. However, for chalcogenides and alkaline iron selenides, and also after including quantum fluctuations, the ratio U/W may increase further, and it may reach the $U/W \sim 1$ threshold widely considered to mark the starting point for a strong coupling description. Note also that the sketch in Fig. 4 is based on our knowledge of the one-orbital Hubbard model, and a proper multiorbital analysis will lead to an even richer phase diagram. In fact, a critical U for the transition between the magnetic metallic state and the magnetic insulating state at low temperatures should also be present, but it is not shown in the sketch for simplicity: this transition should occur at a value of U larger than that given by the pnictides dashed line because these materials are metallic at low temperatures.

In summary, the Fe-based superconductors continue to surprise us with their exotic properties, which do not fit into the simple limits of weak or strong coupling U. Further experimental and theoretical efforts are needed to reveal the secrets of this intriguing family of materials.

Received 13 March 2012; accepted 3 September 2012; published online 3 October 2012

References

1. Bednorz, J. G. & Müller, K. A. Possible high-T_c superconductivity in the Ba–La–Cu–O system. *Z. Phys. B* **64,** 189–193 (1986).
2. Vaknin, D. *et al.* Antiferromagnetism in La_2CuO_{4-y}. *Phys. Rev. Lett.* **58,** 2802–2805 (1987).
3. Tranquada, J. M. *et al.* Neutron-diffraction determination of antiferromagnetic structure of Cu ions in $YBa_2Cu_3O_{6+x}$ with $x = 0.0$ and 0.15. *Phys. Rev. Lett.* **60,** 156–159 (1988).
4. Scalapino, D. J. The case for $d_{x^2-y^2}$ pairing in the cuprate superconductors. *Phys. Rep.* **250,** 329–365 (1995).
5. Dagotto, E. Correlated electrons in high-temperature superconductors. *Rev. Mod. Phys.* **66,** 763–840 (1994).
6. Lee, P. A., Nagaosa, N. & Wen, X-G. Doping a Mott insulator: Physics of high-temperature superconductivity. *Rev. Mod. Phys.* **78,** 17–85 (2006).
7. Fujita, M. *et al.* Progress in neutron scattering studies of spin excitations in high-T_c cuprates. *J. Phys. Soc. Jpn* **81,** 011007 (2012).
8. Johnston, D. C. The puzzle of high temperature superconductivity in layered iron pnictides and chalcogenides. *Adv. Phys.* **59,** 803–1061 (2010).
9. Stewart, G. R. Superconductivity in iron compounds. *Rev. Mod. Phys.* **83,** 1589–1652 (2011).
10. Paglione, J. & Greene, R. L. High-temperature superconductivity in iron-based materials. *Nature Phys.* **6,** 645–658 (2010).
11. Kamihara, Y., Watanabe, T., Hirano, M. & Hosono, H. Iron-based layered superconductor $La[O_{1-x}F_x]FeAs$ ($x = 0.05$–0.12) with $T_c = 26$ K. *J. Am. Chem. Soc.* **130,** 3296–3297 (2008).
12. Rotter, M., Tegel, M. & Johrendt, D. Superconductivity at 38 K in the iron arsenide $(Ba_{1-x}K_x)Fe_2As_2$. *Phys. Rev. Lett.* **101,** 107006 (2008).
13. Chu, C. W. *et al.* The synthesis and characterization of LiFeAs and NaFeAs. *Physica C* **469,** 326–331 (2009).
14. Hsu, F-C. *et al.* Superconductivity in the PbO-type structure α-FeS. *Proc. Natl Acad. Sci. USA* **105,** 14262 (2008).
15. Mazin, I. I. Superconductivity gets an iron boost. *Nature* **464,** 183–186 (2010).
16. Hirschfeld, P. J., Korshunov, M. M. & Mazin, I. I. Gap symmetry and structure of Fe-based superconductors. *Rep. Prog. Phys.* **74,** 124508 (2011).
17. Dong, J. *et al.* Competing orders and spin-density-wave instability in $LaO_{1-x}F_xFeAs$. *Euro. Phys. Lett.* **83,** 27006 (2008).
18. Fawcett, E. Spin-density-wave antiferromagnetism in chromium. *Rev. Mod. Phys.* **60,** 209–283 (1988).
19. De la Cruz, C. *et al.* Magnetic order close to superconductivity in the iron-based layered $LaO_{1-x}F_xFeAs$ systems. *Nature* **453,** 899–902 (2008).
20. Huang, Q. *et al.* Neutron-diffraction measurements of magnetic order and a structural transition in the parent $BaFe_2As_2$ compound of FeAs-based high-temperature superconductors. *Phys. Rev. Lett.* **101,** 257003 (2008).
21. Li, S. *et al.* Structural and magnetic phase transitions in $Na_{1-\delta}FeAs$. *Phys. Rev. B* **80,** 020504 (2009).
22. Mazin, I. I., Johannes, M. D., Boeri, L., Koepernik, K. & Singh, D. J. Problems with reconciling density functional theory calculations with experiment in ferropnictides. *Phys. Rev. B* **78,** 085104 (2008).
23. Kuroki, K. *et al.* Unconventional pairing originating from the disconnected Fermi surfaces of superconducting $LaFeAsO_{1-x}F_x$. *Phys. Rev. Lett.* **101,** 087004 (2008).
24. Chubukov, A. V. Pairing mechanism in Fe-based superconductors. *Annu. Rev. Condens. Matter Phys.* **3,** 57–92 (2012).
25. Wang, F. & Lee, D-H. The electron-pairing mechanism of iron-based superconductors. *Science* **332,** 200–204 (2011).
26. Eschrig, M. The effect of collective spin-1 excitations on electronic spectra in high-T_c superconductors. *Adv. Phys.* **55,** 47–183 (2006).
27. Maier, T. A. & Scalapino, D. J. Theory of neutron scattering as a probe of the superconducting gap in the iron pnictides. *Phys. Rev. B* **78,** 020514 (2008).
28. Korshunov, M. M. & Eremin, I. Theory of magnetic excitations in iron-based layered superconductors. *Phys. Rev. B* **78,** 140509 (2008).
29. Christianson, A. D. *et al.* Resonant spin excitation in the high temperature superconductor $Ba_{0.6}K_{0.4}Fe_2As_2$. *Nature* **456,** 930–932 (2008).
30. Zhang, C. L. *et al.* Neutron scattering studies of spin excitations in hole-doped $Ba_{0.67}K_{0.33}Fe_2As_2$ superconductor. *Sci. Rep.* **1,** 115 (2011).
31. Castellan, J-P. *et al.* Effect of Fermi surface nesting on resonant spin excitations in $Ba_{1-x}K_xFe_2As_2$. *Phys. Rev. Lett.* **107,** 177003 (2011).
32. Lumsden, M. D. *et al.* Two-dimensional resonant magnetic excitation in $BaFe_{1.84}Co_{0.16}As_2$. *Phys. Rev. Lett.* **102,** 107005 (2009).
33. Chi, S. *et al.* Inelastic neutron-scattering measurements of a three-dimensional spin resonance in the FeAs-based $BaFe_{1.9}Ni_{0.1}As_2$ superconductor. *Phys. Rev. Lett.* **102,** 107006 (2009).
34. Inosov, D. S. *et al.* Normal-state spin dynamics and temperature-dependent spin resonance energy in an optimally doped iron arsenide superconductor. *Nature Phys.* **6,** 178 (2010).
35. Park, J. T. *et al.* Symmetry of spin excitation spectra in tetragonal paramagnetic and superconducting phases of 122-ferropnictides. *Phys. Rev. B* **82,** 134503 (2010).
36. Lester, C. *et al.* Dispersive spin fluctuations in the nearly optimally doped superconductor $Ba(Fe_{1-x}Co_x)_2As_2$ ($x = 0.065$). *Phys. Rev. B* **81,** 064505 (2010).
37. Li, H. F. *et al.* Anisotropic and quasipropagating spin excitations in superconducting $Ba(Fe_{0.926}Co_{0.074})_2As_2$. *Phys. Rev. B* **82,** 140503 (2010).
38. Luo, H. Q. *et al.* Electron doping evolution of the anisotropic spin excitations in $BaFe_{2-x}Ni_xAs_2$. *Phys. Rev. B* **86,** 024508 (2012).
39. Mook, H. A. *et al.* Unusual relationship between magnetism and superconductivity in $FeTe_{0.5}Se_{0.5}$. *Phys. Rev. Lett.* **104,** 187002 (2010).
40. Qiu, Y. *et al.* Spin gap and resonance at the nesting wave vector in superconducting $FeSe_{0.4}Te_{0.6}$. *Phys. Rev. Lett.* **103,** 067008 (2009).
41. Lumsden, M. D. *et al.* Evolution of spin excitations into the superconducting state in $FeTe_{1-x}Se_x$. *Nature Phys.* **6,** 182–186 (2010).
42. Richard, P., Sato, T., Nakayama, K., Takahashi, T. & Ding, H. Fe-based superconductors: An angle-resolved photoemission spectroscopy perspective. *Rep. Prog. Phys.* **74,** 124512 (2011).
43. Si, Q. & Abrahams, E. Strong correlations and magnetic frustration in the high T_c iron pnictides. *Phys. Rev. Lett.* **101,** 076401 (2008).
44. Si, Q., Abrahams, E., Dai, J. H. & Zhu, J-X. Correlation effects in the iron pnictides. *New J. Phys.* **11,** 045001 (2009).
45. Fang, C., Yao, H., Tsai, W. F., Hu, J. P. & Kivelson, S. A. Theory of electron nematic order in LaOFeAs. *Phys. Rev. B* **77,** 224509 (2008).

46. Xu, C. K., Müller, M. & Sachdev, S. Ising and spin orders in the iron-based superconductors. *Phys. Rev. B* **78,** 020501 (2008).
47. Seo, K., Bernevig, B. A. & Hu, J. P. Pairing symmetry in a two-orbital exchange coupling model of oxypnictides. *Phys. Rev. Lett.* **101,** 206404 (2008).
48. Fang, C. *et al.* Robustness of *s*-wave pairing in electron overdoped $A_{1-y}Fe_{2-x}Se_2$. *Phy. Rev. X* **1,** 011009 (2011).
49. Nicholson, A. *et al.* Competing pairing symmetries in a generalized two-orbital model for the pnictide superconductors. *Phys. Rev. Lett.* **106,** 217002 (2011).
50. Guo, J. G. *et al.* Superconductivity in the iron selenide $K_xFe_2Se_2$ ($0 \leq x \leq 1.0$). *Phys. Rev. B* **82,** 180520 (2010).
51. Fang, M. H. *et al.* Fe-based high temperature superconductivity with $T_c = 31$ K bordering an insulating antiferromagnet in $(Tl,K)Fe_xSe_2$ Crystals. *Europhys. Lett.* **94,** 27009 (2011).
52. Wang, X-P. *et al.* Strong nodeless pairing on separate electron Fermi surface sheets in $(Tl,K)Fe_{1.78}Se_2$ probed by ARPES. *Europhys. Lett.* **93,** 57001 (2011).
53. Zhang, Y. *et al.* Heavily electron-doped electronic structure and isotropic superconducting gap in $A_xFe_2Se_2$ (A = K, Cs). *Nature Mater.* **10,** 273–277 (2011).
54. Mou, D. *et al.* Distinct Fermi surface topology and nodeless superconducting gap in a $(Tl_{0.58}Rb_{0.42})Fe_{1.72}Se_2$ superconductor. *Phys. Rev. Lett.* **106,** 107001 (2011).
55. Bao, W. *et al.* A novel large moment antiferromagnetic order in $K_{0.8}Fe_{1.6}Se_2$ superconductor. *Chinese Phys. Lett.* **28,** 086104 (2011).
56. Ye, F. *et al.* Common crystalline and magnetic structure of superconducting $A_2Fe_4Se_5$ (A = K,Rb,Cs,Tl) single crystals measured using neutron diffraction. *Phys. Rev. Lett.* **107,** 137003 (2011).
57. Qazilbash, M. M. *et al.* Electronic correlations in the iron pnictides. *Nature Phys.* **5,** 647–650 (2009).
58. Haule, K., Shim, J. H. & Kotliar, G. Correlated electronic structure of $LaO_{1-x}F_xFeAs$. *Phys. Rev. Lett.* **100,** 226402 (2008).
59. Coldea, R. *et al.* Spin waves and electronic interactions in La_2CuO_4. *Phys. Rev. Lett.* **86,** 5377–5380 (2001).
60. Headings, N. S., Hayden, S. M., Coldea, R. & Perring, T. G. Anomalous high-energy spin excitations in the high-T_c superconductor-parent antiferromagnet La_2CuO_4. *Phys. Rev. Lett.* **105,** 247001 (2010).
61. Fang, M. H. *et al.* Superconductivity close to magnetic instability in $Fe(Se_{1-x}Te_x)_{0.82}$. *Phys. Rev. B* **78,** 224503 (2008).
62. Subedi, A., Zhang, L. J., Dingh, D. J. & Du, M. H. Density functional study of FeS, FeSe, and FeTe: Electronic structure, magnetism, phonons, and superconductivity. *Phys. Rev. B* **78,** 134514 (2008).
63. Bao, W. *et al.* Tunable $(\delta\pi, \delta\pi)$-type antiferromagnetic order in α-Fe(Te,Se) superconductors. *Phys. Rev. Lett.* **102,** 247001 (2009).
64. Li, S. L. *et al.* First-order magnetic and structural phase transitions in $Fe_{1+y}Se_xTe_{1-x}$. *Phys. Rev. B* **79,** 054503 (2009).
65. Diallo, S. O. *et al.* Itinerant magnetic excitations in antiferromagnetic $CaFe_2As_2$. *Phys. Rev. Lett.* **102,** 187206 (2009).
66. Zhao, J. *et al.* Spin waves and magnetic exchange interactions in $CaFe_2As_2$. *Nature Phys.* **5,** 555–560 (2009).
67. Ewings, R. A. *et al.* Itinerant spin excitations in $SrFe_2As_2$ measured by inelastic neutron scattering. *Phys. Rev. B* **83,** 214519 (2011).
68. Harriger, L. W. *et al.* Nematic spin fluid in the tetragonal phase of $BaFe_2As_2$. *Phys. Rev. B* **84,** 054544 (2011).
69. Rodriguez, E. E. *et al.* Magnetic-crystallographic phase diagram of the superconducting parent compound $Fe_{1+x}Te$. *Phys. Rev. B* **84,** 064403 (2011).
70. Lipscombe, O. J. *et al.* Spin waves in the $(\pi, 0)$ magnetically ordered iron chalcogenide $Fe_{1.05}Te$. *Phys. Rev. Lett.* **106,** 057004 (2011).
71. Zaliznyak, I. A. *et al.* Unconventional temperature enhanced magnetism in iron telluride. *Phys. Rev. Lett.* **107,** 216403 (2011).
72. Wang, M. Y. *et al.* Spin waves and magnetic exchange interactions in insulating $Rb_{0.89}Fe_{1.58}Se_2$. *Nature Commun.* **2,** 580 (2011).
73. Ni, N. *et al.* Effects of Co substitution on thermodynamic and transport properties and anisotropic H_{c2} in $Ba(Fe_{1-x}Co_x)_2As_2$ single crystals. *Phys. Rev. B* **78,** 214515 (2008).
74. Chu, J-H. *et al.* Determination of the phase diagram of the electron-doped superconductor $Ba(Fe_{1-x}Co_x)_2As_2$. *Phys. Rev. B* **79,** 014506 (2009).
75. Lester, C. *et al.* Neutron scattering study of the interplay between structure and magnetism in $Ba(Fe_{1-x}Co_x)_2As_2$. *Phys. Rev. B* **79,** 144523 (2009).
76. Pratt, D. K. *et al.* Coexistence of competing antiferromagnetic and superconducting phases in the underdoped $Ba(Fe_{0.953}Co_{0.047})_2As_2$ compound using X-ray and neutron scattering techniques. *Phys. Rev. Lett.* **103,** 087001 (2009).
77. Christianson, A. D. *et al.* Static and dynamic magnetism in underdoped superconductor $BaFe_{1.92}Co_{0.08}As_2$. *Phys. Rev. Lett.* **103,** 087002 (2009).
78. Wang, M. Y. *et al.* Electron-doping evolution of the low-energy spin excitations in the iron arsenide superconductor $BaFe_{2-x}Ni_xAs_2$. *Phys. Rev. B* **81,** 174524 (2010).
79. Wang, M. Y. *et al.* Magnetic field effect on static antiferromagnetic order and spin excitations in the underdoped iron arsenide superconductor $BaFe_{1.92}Ni_{0.08}As_2$. *Phys. Rev. B* **83,** 094516 (2011).
80. Pratt, D. K. *et al.* Incommensurate spin-density wave order in electron-doped $BaFe_2As_2$ superconductors. *Phys. Rev. Lett.* **106,** 257001 (2011).
81. Luo, H. Q. *et al.* Coexistence and competition of the short-range incommensurate antiferromagnetic order with the superconducting state of $BaFe_{2-x}Ni_xAs_2$. *Phys. Rev. Lett.* **108,** 247002 (2012).
82. Nandi, S. *et al.* Anomalous suppression of the orthorhombic lattice distortion in superconducting $Ba(Fe_{1-x}Co_x)_2As_2$ single crystals. *Phys. Rev. Lett.* **104,** 057006 (2010).
83. Chen, H. *et al.* Coexistence of the spin-density wave and superconductivity in $Ba_{1-x}K_xFe_2As_2$. *Europhys. Lett.* **85,** 17006 (2009).
84. Park, J. T. *et al.* Electronic phase separation in the slightly underdoped iron pnictide superconductor $Ba_{1-x}K_xFe_2As_2$. *Phys. Rev. Lett.* **102,** 117006 (2009).
85. Avci, S. *et al.* Magnetoelastic coupling in the phase diagram of $Ba_{1-x}K_xFe_2As_2$ as seen via neutron diffraction. *Phys. Rev. B* **83,** 172503 (2011).
86. Wiesenmayer, E. *et al.* Microscopic coexistence of superconductivity and magnetism in $Ba_{1-x}K_xFe_2As_2$. *Phys. Rev. Lett.* **107,** 237001 (2011).
87. Graser, S. *et al.* Spin fluctuations and superconductivity in a three-dimensional tight-binding model for $BaFe_2As_2$. *Phys. Rev. B* **81,** 214503 (2010).
88. Zhang, J. H., Sknepnek, R. & Schmalian, J. Spectral analysis for the iron-based superconductors: Anisotropic spin fluctuations and fully gapped $s^{\pm}$-wave superconductivity. *Phys. Rev. B* **82,** 134527 (2010).
89. Liu, M. S. *et al.* Nature of magnetic excitations in superconducting $BaFe_{1.9}Ni_{0.1}As_2$. *Nature Phys.* **8,** 376–381 (2012).
90. Lee, C. H. *et al.* Incommensurate spin fluctuations in hole-overdoped superconductor KFe_2As_2. *Phys. Rev. Lett.* **106,** 067003 (2011).
91. Park, H., Haule, K. & Kotliar, G. Magnetic excitation spectra in $BaFe_2As_2$: A two-particle approach within a combination of the density functional theory and the dynamical mean-field theory method. *Phys. Rev. Lett.* **107,** 137007 (2011).
92. Terashima, T. *et al.* Fermi surface and mass enhancement in KFe_2As_2 from de Haas-van Alphen effect measurements. *J. Phys. Soc. Jpn* **79,** 053702 (2010).
93. Rourke, P. M. C. *et al.* A detailed de Haas–van Alphen effect study of the overdoped cuprate $Tl_2Ba_2CuO_{6+\delta}$. *New J. Phys.* **12,** 105009 (2010).
94. Nakamura, K., Arita, R. & Imada, M. *Ab initio* derivation of low-energy model for iron-based superconductors LaFeAsO and LaFePO. *J. Phys. Soc. Jpn* **77,** 093711 (2008).
95. Inosov, D. S. *et al.* Crossover from weak to strong pairing in unconventional superconductors. *Phys. Rev. B* **83,** 214520 (2011).
96. Yin, Z. P., Haule, K. & Kotliar, G. Kinetic frustration and the nature of the magnetic and paramagnetic states in iron pnictides and iron chalcogenides. *Nature Mater.* **10,** 932–935 (2011).
97. He, C. *et al.* Electronic-structure-driven magnetic and structure transitions in superconducting NaFeAs single crystals measured by angle-resolved photoemission spectroscopy. *Phys. Rev. Lett.* **105,** 117002 (2010).
98. Luo, Q. *et al.* Neutron and ARPES constraints on the couplings of the multiorbital Hubbard model for the iron pnictides. *Phys. Rev. B* **82,** 104508 (2010).
99. Daghofer, M., Nicholson, A., Moreo, A. & Dagotto, E. Three-orbital model for the iron-based superconductors. *Phys. Rev. B* **81,** 014511 (2010).
100. Kubo, K. & Thalmeier, P. Correlation effects on antiferromagnetism in Fe pnictides. *J. Phys. Soc. Jpn* **80,** SA121 (2011).
101. Miyake, T., Nakamura, K., Arita, R. & Imada, M. Comparison of *ab initio* low-energy models for LaFePO, BaFe2As2, LiFeAs, FeSe, and FeTe: Electron correlation and covalency. *J. Phys. Soc. Jpn* **79,** 044705 (2010).
102. Johannes, M. D. & Mazin, I. I. Microscopic origin of magnetism and magnetic interactions in ferropnictides. *Phys. Rev. B* **79,** 220510 (2009).
103. Haule, K. & Kotliar, G. Coherence–incoherence crossover in the normal state of iron oxypnictides and importance of Hund's rule coupling. *New J. Phys.* **11,** 025021 (2009).
104. Lv, W. L., Krüger, F. & Phillips, P. Orbital ordering and unfrustrated $(\pi, 0)$ magnetism from degenerate double exchange in the iron pnictides. *Phys. Rev. B* **82,** 045125 (2010).
105. Yin, W-G., Lee, C. C. & Ku, W. Unified picture for magnetic correlations in iron-based superconductors. *Phys. Rev. Lett.* **105,** 107004 (2010).
106. Shimojima, T. *et al.* Orbital-dependent modifications of electronic structure across the magnetostructural transition in $BaFe_2As_2$. *Phys. Rev. Lett.* **104,** 057002 (2010).
107. Daghofer, M. *et al.* Orbital-weight redistribution triggered by spin order in the pnictides. *Phys. Rev. B* **81,** 180514 (2010).
108. Fisher, I. R., Degiorgi, L. & Shen, Z. X. In-plane electronic anisotropy of underdoped '122' Fe-arsenide superconductors revealed by measurements of detwinned single crystals. *Rep. Prog. Phys.* **74,** 124506 (2011).
109. Tanatar, M. A. *et al.* Uniaxial-strain mechanical detwinning of $CaFe_2As_2$ and $BaFe_2As_2$ crystals: Optical and transport study. *Phys. Rev. B* **81,** 814508 (2010).
110. Zhang, X. T. & Dagotto, E. Anisotropy of the optical conductivity of a pnictide superconductor from the undoped three-orbital Hubbard model. *Phys. Rev. B* **84,** 132505 (2011).

111. Fradkin, E., Kivelson, S. A., Lawler, M. J., Eisenstein, J. P. & Mackenzie, A. P. Nematic Fermi fluids in condensed matter physics. *Annu. Rev. Condens. Matter Phys.* **1,** 153–178 (2010).
112. Yi, M. *et al.* Symmetry breaking orbital anisotropy on detwinned $Ba(Fe_{1-x}Co_x)_2As_2$ above the spin density wave transition. *Proc. Natl Acad. Sci. USA* **108,** 6878 (2011).
113. Nakajima, M. *et al.* Unprecedented anisotropic metallic state in undoped iron arsenide $BaFe_2As_2$ revealed by optical spectroscopy. *Proc. Natl Acad. Sci. USA* **108,** 12238 (2011).
114. Dhital, C. *et al.* Effect of uniaxial strain on the structural and magnetic phase transitions in $BaFe_2As_2$. *Phys. Rev. Lett.* **108,** 087001 (2012).
115. Kasahara, S. *et al.* Electronic nematicity above the structural and superconducting transition in $BaFe_2(As_{1-x}P_x)_2$. *Nature* **486,** 382–385 (2012).
116. Fernandes, R. M., Chubukov, A. V., Knolle, J., Eremin, I. & Schmalian, J. Preemptive nematic order, pseudogap, and orbital order in the iron pnictides. *Phys. Rev. B* **85,** 024534 (2012).
117. Gretarsson, H. *et al.* Revealing the dual nature of magnetism in iron pnictides and iron chalcogenides using *x*-ray emission spectroscopy. *Phys. Rev. B* **84,** 100509 (2011).
118. Bondino, F. *et al.* Evidence for strong itinerant spin fluctuations in the normal state of $CeFeAsO_{0.89}F_{0.11}$ iron-oxypnictide superconductors. *Phys. Rev. Lett.* **101,** 267001 (2008).
119. Hansmann, P. *et al.* Dichotomy between large local and small ordered magnetic moments in iron-based superconductors. *Phys. Rev. Lett.* **104,** 197002 (2010).
120. Shimojima, T. *et al.* Orbital-independent superconducting gaps in iron pnictides. *Science* **332,** 564–567 (2011).
121. Moreo, A. *et al.* Properties of a two-orbital model for oxypnictide superconductors: Magnetic order, B_{2g} spin-singlet pairing channel, and its nodal structure. *Phys. Rev. B* **79,** 134502 (2009).
122. Nicholson, A. *et al.* Role of degeneracy, hybridization, and nesting in the properties of multi-orbital systems. *Phys. Rev. B* **84,** 094519 (2011).
123. Arnold, B. J. *et al.* Nesting of electron and hole Fermi surfaces in nonsuperconducting $BaFe_2P_2$. *Phys. Rev. B* **83,** 220504 (2011).
124. Borisenko, S. V. *et al.* Superconductivity without nesting in LiFeAs. *Phys. Rev. Lett.* **105,** 067002 (2010).
125. Qian, T. *et al.* Absence of holelike Fermi surface in superconducting $K_{0.8}Fe_{1.7}Se_2$ revealed by ARPES. *Phys. Rev. Lett.* **106,** 187001 (2011).
126. Chuang, T-M. *et al.* Nematic electronic structure in the parent state of the iron-based superconductor $Ca(Fe_{1-x}Co_x)_2As_2$. *Science* **327,** 181–184 (2010).
127. Arita, R. & Ikeda, H. Is Fermi-surface nesting the origin of superconductivity in iron pnictides?: A fluctuation-exchange-approximation study. *J. Phys. Soc. Jpn* **78,** 113707 (2009).
128. Dagotto, E., Hotta, T. & Moreo, A. Colossal magnetoresistant materials: The key role of phase separation. *Phys. Rep.* **344,** 1–153 (2001).
129. Daghofer, M., Nicholson, A. & Moreo, A. Spectral density in a nematic state of iron pnictides. *Phys. Rev. B* **85,** 184515 (2012).

Acknowledgements

We thank L. W. Harriger for preparing the figures shown in this manuscript. We are also grateful to T. A. Maier for calculating the FSs of $BaFe_2As_2$ shown in Fig. 2d. P.D. is supported by the US NSF DMR-1063866 (neutron scattering studies on electron-doped iron pnictides), OISE-0968226 (international collaboration) and by US DOE, BES, under Grant No. DE-FG02-05ER46202 (single crystal growth at UTK and neutron scattering studies of hole-doped iron pnictides and other iron-based superconductors). Work at Institute of Physics is supported by the Ministry of Science and Technology of China 973 program (2012CB821400). E.D. is supported by the US DOE, BES, Materials Sciences and Engineering Division and by the US NSF DMR-11-04386.

Author contributions

P.D. and E.D. wrote the experimental and theoretical portions of the article, respectively. J.P.H. revised the article. All authors discussed the outline of the article.

Additional information

Reprints and permissions information is available online at www.nature.com/reprints. Correspondence and requests for materials should be addressed to P.D. or E.D.

Competing financial interests

The authors declare no competing financial interests.